Ndukwe, I. E., Shchukina, A., Kazimierczuk, K., Cobas, C., & Butts, C. P. (2016). EXtended ACquisition Time (EXACT) NMR: A Case for 'Burst' Non-Uniform Sampling. *ChemPhysChem*, *17*(18), 2799-2803. https://doi.org/10.1002/cphc.201600541

CHEMPHYSCHEM

Supporting Information

EXtended ACquisition Time (EXACT) NMR—A Case for ′Burst′ Non-Uniform Sampling

Ikenna E. Ndukwe,[a] Alexandra Shchukina,[b, c] Krzysztof Kazimierczuk,[b] Carlos Cobas,[d] and Craig P. Butts*[a]

cphc_201600541_sm_miscellaneous_information.pdf

EXtended ACquisition Time (EXACT) NMR – A case for 'Burst' Non-Uniform Sampling

Ikenna E. Ndukwe, Alexandra Shchukina, Krzysztof Kazimierczuk, Carlos Cobas and Craig P. Butts*

Supporting Information

1.1 Experimental

All experiments were performed on a freshly prepared strychnine sample of 30 mg/0.7 ml $CDCl_3$ on a Varian VNMRS 500 MHz Direct Drive Spectrometer with Agilent OneNMR probe and experiments acquired at 25°C. All data were collected with a recovery delay of 1 second and processed with an unshifted Gaussian window function along the indirect dimension for 2D experiments, while missing data points in the direct dimension and in 1D experiments were reconstructed with two different implementations of IST algorithm. Firstly, as implemented in the *mddnmr 2.4* package (see www.mddnmr.spektrino.com). This version was adapted to processing 1D datasets or the direct dimension of multidimensional NMR experiments by a Python wrapper written by Alexandra Shchukina and Krzysztof Kazimierczuk (co-authors of this manuscript), where virtual echo option was included.[1] Secondly, the data were also reconstructed in Mestrenova written by Carlos Cobas (also a co-author). The following parameters were used for reconstructing/processing the spectra shown in this manuscript;

1. EXACT ^{13}C spectra: 200 iterations were used and threshold was set to 0.9 of the spectral maximum in each iteration. Spectral width was 31,250 Hz, centred at 110 ppm. 32,768 complex points obtained from a 16K measured FID (50 % sampling density) after IST reconstruction of missing data points was zero-filled to 65,536.
2. EXACT HSQC spectrum: 200 iterations were used and threshold was set to 0.9 of the spectral maximum in each iteration. ^{1}H and ^{13}C spectral widths were of 10,000Hz and 25,125.6 Hz respectively, centred at 5 ppm in F_2 and 90 ppm in F_1. The chunk size was varied within the FID from 15-88 ms and with gaps of Δ=22 ms or 25 ms between data chunks. 8000 * 96 (F_2 * F_1) complex points were obtained after IST reconstruction in F_2 (55 % sampling in F_2) and zero-filled to 16384 * 2048 (FID shown in Figure S8 on page 7).
3. HSQC spectrum: ^{1}H and ^{13}C spectral widths were 10,000Hz and 25,125.6 Hz respectively, centred at 5 ppm in F_2 and 90 ppm in F_1. 4000 * 96 (F_2 * F_1) acquired complex points were extrapolated by linear prediction to 8192 in F_2 followed by zero-filling to 16384 * 2048.
4. EXACT pure shift EXSIDE: The inter-pulse delay, τ, during the INEPT periods was optimized for $^{n}J_{CH}$ = 8 Hz. Data were acquired with ^{1}H and ^{13}C spectral widths of 10,000 Hz and 10051.5 Hz respectively and centred at 5.0 ppm in F_2 and 40 ppm in F_1. Two scans of 3300 complex points (chunk = 0.016 s and $\Delta \approx 0.012$ s – here Δ includes region selective inversion WURST2i pulse[2]) for each t_1 increment out of a total of 670. The acquired data was processed with IST algorithm to reconstruct missing data points in the directly detected dimension. An unshifted Gaussian function in the indirect dimension gave the spectrum of total size 4096 * 4096 (t_1 * t_2) after zero filling. A *J* – scaling factor, N, of 15 was used in these experiments giving an average experimental run time of 1½ hrs. The length of data acquired per chunk during the windowed acquisition period of the EXACT pure shift

EXSIDE sequence (Figure S3) is limited to < $1/(3 * {}^{n}J_{HH})$ (where n = 2, 3) but can be modified as required.

5. EXSIDE pure shift: Same ^{1}H and ^{13}C spectral width as above, in (4), but two scans of 1600 complex points for each t_1 increments of a total of 670. Total spectral size after processing with unshifted Gaussian in F_1 and zero filling is 4096 * 4096.
6. EXSIDE: Same acquisition parameters and processing as (5) above.

NOTE REGARDING LENGTHS OF CHUNKS/GAPS IN EXACT FIDS: The timings of chunk and gap lengths cannot be made completely random as one is limited by maximum and minimum limits on the length of pulses and any delays placed within the gaps. However within those limits these time periods were set to a range of arbitrary values, varying from chunk to chunk within each scan.

****

Duty cycle is calculated thus:

$$Duty\ Cycle\ (\%) = \frac{AT}{Recycle\ time} * 100\ \%$$

AT = Duration of data sampling periods (does not include gaps)
Recycle time = Relaxation delay + total acquisition time (including gaps)

****

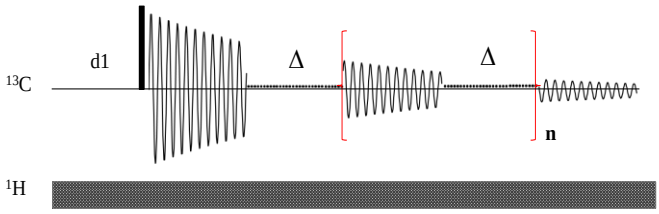

Figure S1: An EXACT ^{13}C{^{1}H} pulse acquire experiment with the slim filled box an excitation pulse of 45° tip angle. d1 = recycle delay.

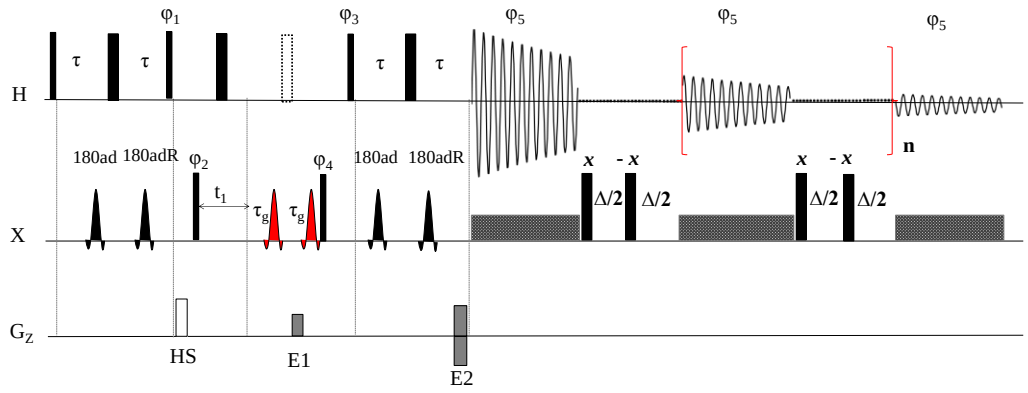

Figure S2: The EXACT-HSQC pulse sequence with 180° and 90° pulses represented as wide and narrow filled boxes respectively. The unfilled box with dotted lines is a 180° pulse turned-on if multiplicity editing is required. Shaped pulses are ^{13}C broadband adiabatic (black and red) inversion pulses. INEPT delays are $\tau = 1/(4 * {}^{1}J_{CH})$ and $\tau_g = 1/(2 * {}^{1}J_{CH})$ where ${}^{1}J_{CH} = 146Hz$. The phase cycle are; ϕ_1 = *y, y, -y, -y,* ϕ_2 = *x, -x,* ϕ_3 = *x, x, x, x, -x, -x, -x, -x,* ϕ_4 = *x, x, x, x, x, x, x, x, -x, -x, -x, -x, -x, -x, -x, -x,* ϕ_5 = *y, -y, -y, y, -y, y, y, -y, -y, y, y, -y, y, -y, -y, y*. Pulses whose phases are not shown have an *x* phase. The pulse field gradients are shown in the G_Z line as rectangular filled and unfilled boxes and coherence selection for desired ^{1}H – ^{13}C correlation is achieved with a 2.0ms (E1) and 1.0 ms (E2) encoding/decoding gradients, whose power ratio, E1:E2, is set to 1:7.95 (1060:8430.21 dB in this case). HS is a 1.0 ms homospoil gradient of power 1272 dB. Within each scan, the chunk size was varied from 15-88 ms and gaps were varied between Δ=22 ms or 25 in no particular pattern.

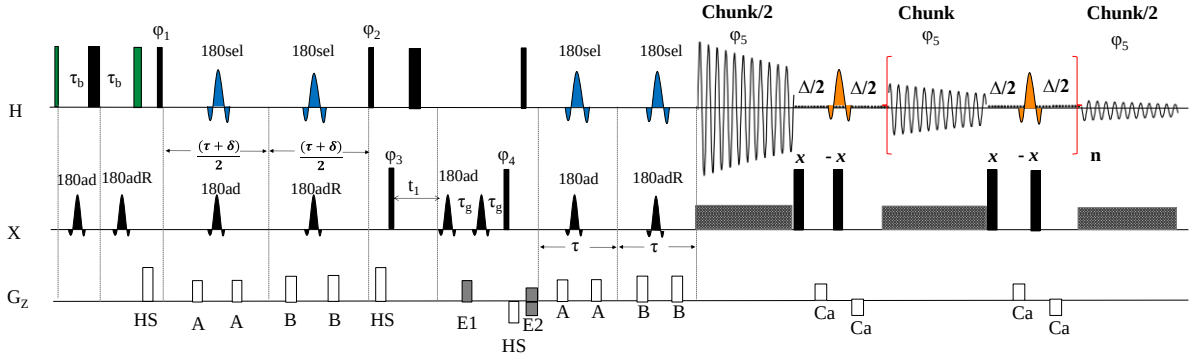

Figure S3: The EXACT pure shift EXSIDE sequence with 180° and 90° pulses represented as wide and narrow filled boxes respectively. Thick and slim green boxes are 135° and 45° pulses respectively whereas shaped pulses are active spin ^{1}H selective q3 (blue) and passive spins WURST2i (orange) and ^{13}C broadband adiabatic (black) inversion pulses. Delays are; $\tau = 1/(4 * {}^{n}J_{CH})$, $\tau_b = 1/(2 * {}^{1}J_{CH})$, τ_g = (encoding gradient duration + recovery delay) and $\delta = t_1 * J - scalingfactor$. Where ${}^{n}J_{CH} = 8Hz$, ${}^{1}J_{CH} = 146Hz$ and J = 15 in this instance. The phase cycles are; ϕ_1 = *x, x, -x, -x,* ϕ_2 = *y,* ϕ_3 = *x, -x,* ϕ_4 = *x, x, x, x, -x, -x, -x, -x,* ϕ_5 = *x, -x, -x, x, -x, x, x, -x*. Pulses whose phases are not shown have an *x* phase. The pulse field gradients are shown in the G_Z line as rectangular filled and unfilled boxes and coherence selection for desired ^{1}H – ^{13}C correlation is achieved with a 2.0ms (E1) and 1.0 ms (E2) encoding/decoding gradients, whose power ratio, E1:E2, is set to 1.99:1 (1060:533.271 dB in this case). HS is a 1.0 ms homospoil gradient of power, 1272 dB which causes rapid relaxation of transverse magnetization present. Gradients 'A' and 'B' are 1.0 ms frequency dephasing/rephasing gradients of power 848 and 1272 dB respectively whereas gradient 'Ca' is 500 µs long of power 250 dB. The duration of the 90° pulse was 7.6 µs (power, 57 dB) and 9.8 µs (power, 53 dB) for ^{1}H and ^{13}C nuclei respectively. The adiabatic ^{13}C 180° pulse (denoted 180ad and 180adR) is a wurst2i swept pulse of duration 465.4 µs and power 48 dB.

1.2 Burst NUS and Reconstruction

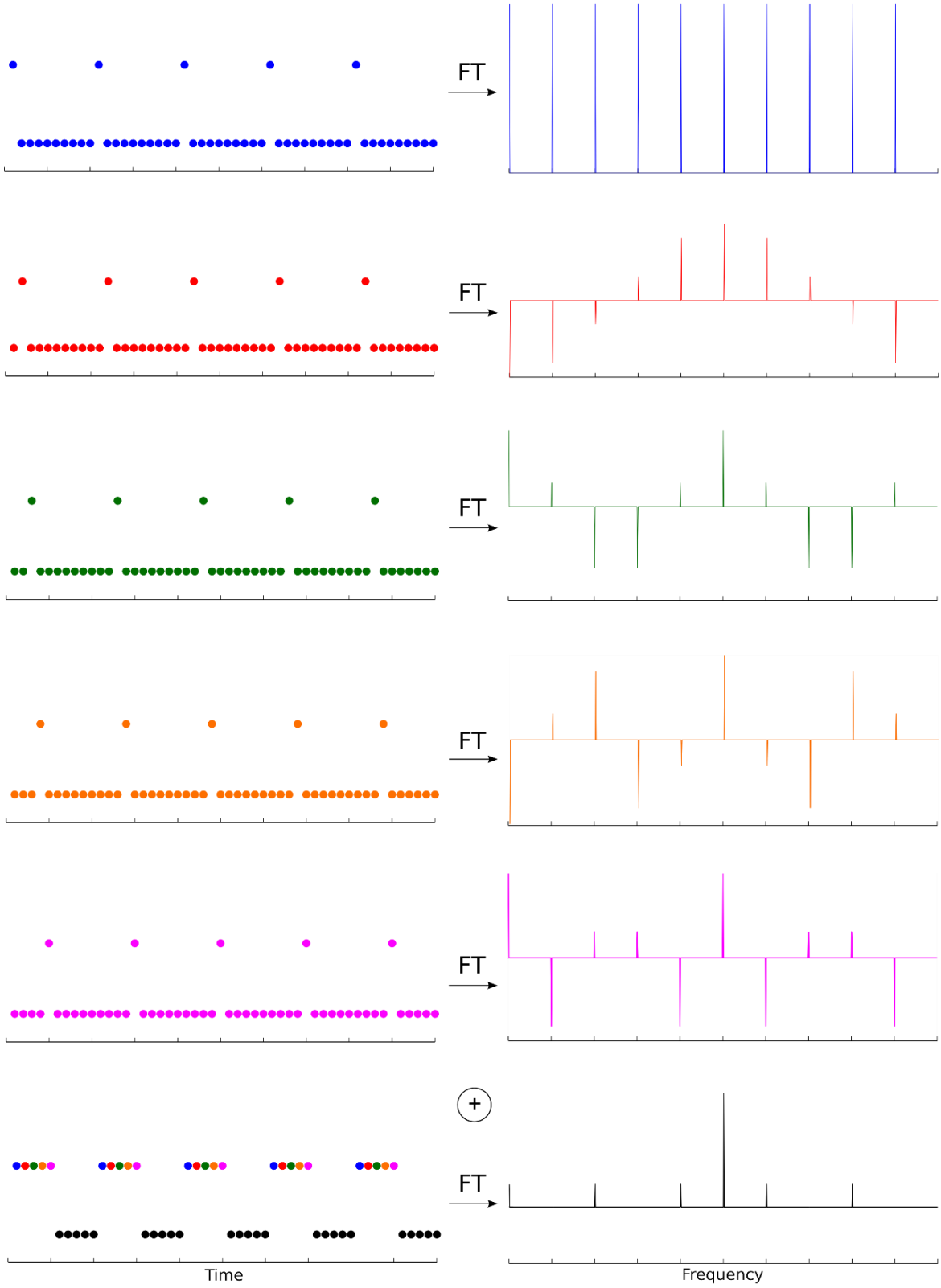

Figure S4: Burst sampling as a sum of regular non-uniformly sampled data points (left) and corresponding Fourier transform artefact pattern (PSF)

Burst sampling used in this manuscript can be treated as a special type of NUS that is described as a superposition of several regular sampling schedules, each being below Nyquist rate and each shifted by one point (Figure S4). Generally, an important condition of recovery of missing points in a NUS data record, besides sparsity of a spectrum (which describes the number of significant spectral points or peaks), is the low coherence of the undersampled Fourier transform matrix. The coherence of an undersampled FT matrix is defined as a maximum among scalar products of all pairs of its columns.[3] This coherence is lowest when sampling points are selected purely at random from the full sampling grid. A visual representation of the coherence in NUS data records is provided by the point spread function (PSF) – a Fourier transformation of the sampling scheme. In fully sampled data, PSF is just a perfect peak ("delta pseudo-function") – the coherence between any two frequencies up to the Nyquist frequency is zero. Whereas in a purely random sampling scheme (shown in Figure S5), the PSF in addition, contains noise-like artefact patterns whose heights corresponds to the coherence between frequencies sampled using a given scheme.

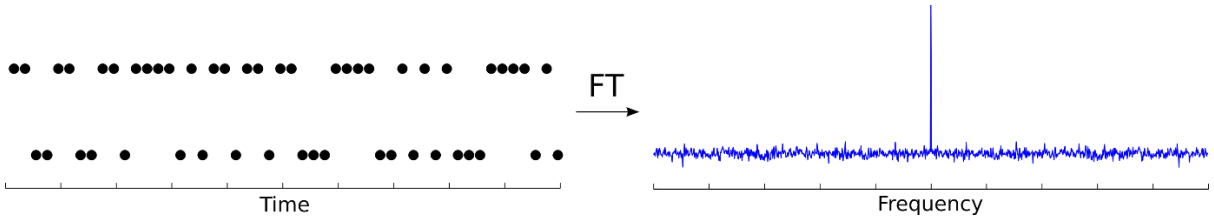

Figure S5: A computed random sampling NUS scheme and its point spread function.

Practically all NUS reconstruction methods start from a spectrum convolved with PSF and attempt to deconvolve the artefact pattern by iterative search for highest peaks. Thus, it is important to distinguish between peaks and artefacts in each of the iterations. The task is relatively easy in case of random NUS, when noise-like artefacts are evenly distributed, but can be more problematic in the burst sampling scheme where regularity of a sampling is introduced. As shown in Figure S4, burst sampling artefacts are "peaky", as the coherence of the inverse FT matrix is high. Experimentally, the artefactual spectrum derived from the FT of a NUS data record is a PSF convoluted with Lorentzian peaks and is shown in Figure S6. The resulting intensities of these false peaks (aliases) are relatively high and thus problematic for the reconstruction algorithms if the length of the sampled data chunks (sampling density) is not large enough compared to the missing data points. Experimental results shown in Figure S7 show an inverse relationship between sampling density and the intensity of the NUS sampling artefacts. It is, however, possible to recover missing data points in burst sampling schemes by using sparsity-enforcing reconstruction algorithms like IST.

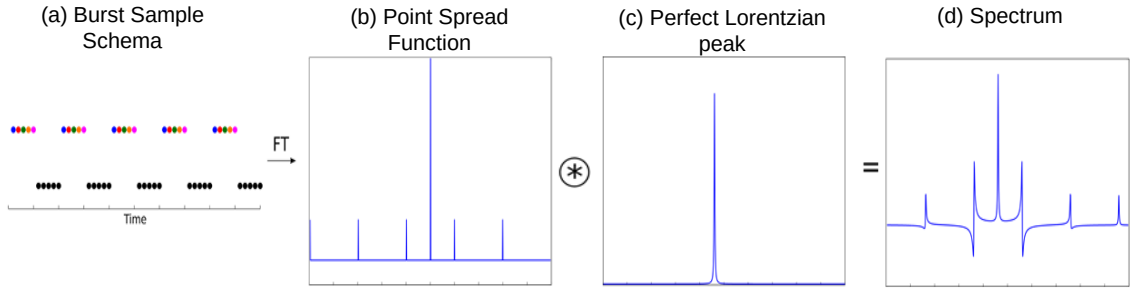

Figure S6: The computed spectrum (far right) of a singlet resonance arising from convolution of a perfect Lorentzian peak with the point spread function of a burst sampling schema analogous to that used in Figure 2b (main text).

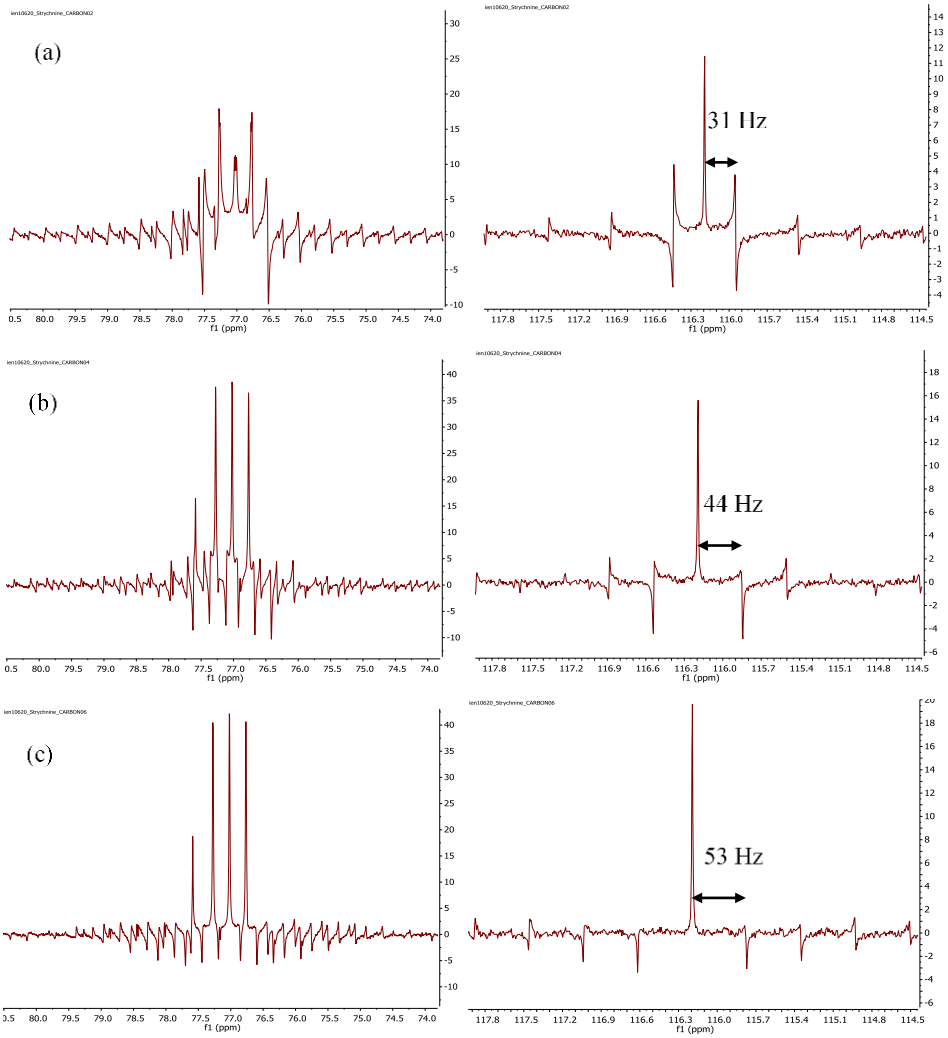

Figure S7: The convoluted PSF of different sampling schedules acquired with the pulse sequence of Figure 1a (main text) showing solvent peak at 77 ppm (with a single resonance by the side) and a singlet peak at 116 ppm. The sampling densities for the spectrum are (a) 50 % sampling – chunk = 16 ms and Δ = 16 ms, (b) 70% sampling – chunk = 16 ms and Δ = 7 ms and (c) 85% sampling – chunk = 16 ms and Δ = 3 ms.

1.3 EXACT HSQC FID

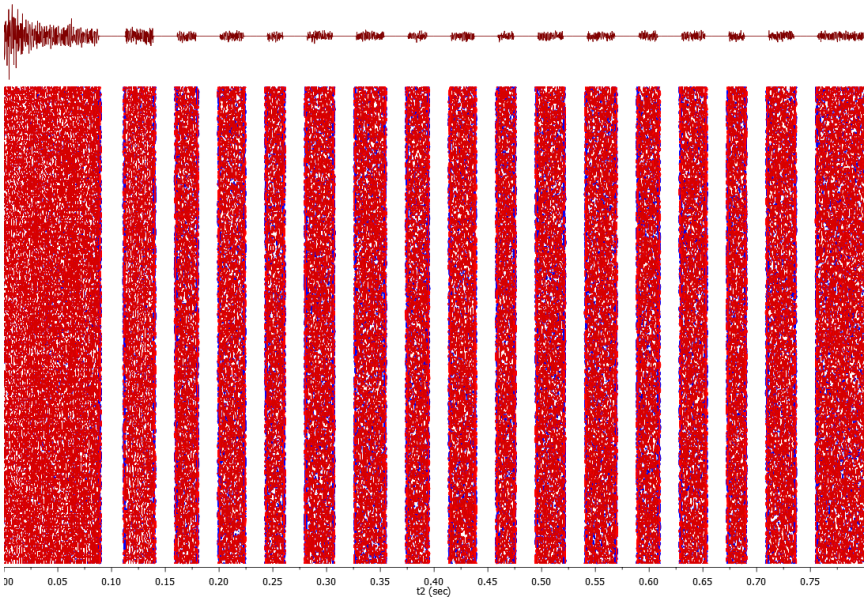

Figure S8: A 0.8 s EXACT HSQC acquisition data showing a trace FID at the top. The sizes of the chunk and gaps have been partially randomized. Sampling density is 55 % with partially randomized chunks of duration ranging from 15 – 88 ms between regular gaps of 22 ms (excluding the first gap, which is 25 ms).

[1] M. Mayzel, K. Kazimierczuk, V. Y. Orekhov, *Chemical Communications* **2014**, *50*, 8947-8950.

[2] E. Kupce, R. Freeman, *Journal of Magnetic Resonance, Series A* **1995**, *115*, 273-276.

[3] H. R. Simon Foucart, *A Mathematical Introduction to Compressive Sensing*, Springer Science+Business Media, New York, **2013**.